2011 American Control Conference
on O'Farrell Street, San Francisco, CA, USA
June 29 - July 01, 2011

# Following Straight Line and Orbital Paths with Input Constraints

Randal W. Beard and Jeffrey Humpherys

*Abstract*— **This paper considers the problem of fixed wing unmanned air vehicles following straight lines and orbits. To account for ambient winds, we use a path following approach as opposed to trajectory tracking. The unique feature of this paper is that we explicitly account for roll angle constraints and flight path angle constraints. The guidance laws are derived using the theory of nested saturations.**

## I. Introduction

Many application of small and miniature UAVs require that the vehicle traverse a particular inertially defined path. For example, the UAV may be required to survey a series of geographic features where the objective is to record images of the features. In these applications, it is important that the UAV be on the path, but the time parameterization of the path is not critical. One approach to this problem is to impose a time parameterization of the path and to pose the associated trajectory tracking problem. However, this approach is not well suited to small and miniature fixed wing UAVs since the ambient wind can be a significant percentage of the airspeed of the vehicle.

Fixed wing vehicles are typically designed to fly at a particular airspeed that maximizes the fuel efficiency. However flying at a constant airspeed is not compatible with trajectory tracking in wind. For example, consider the case where the desired path is a circular orbit and there is a strong ambient wind. If the time parameterization calls for a constant speed with respect to the ground, then airspeed will need to increase significantly when the vehicle is heading into the wind, and will need to decrease significantly when the vehicle is heading downwind. Not only do these large variations in the airspeed destroy the fuel efficiency, they can also cause the vehicle to stall in downwind conditions.

An alternative to trajectory tracking is path following where the vehicle attempts to regulate is distance from the geometric path, as opposed to regulate the error from a time varying trajectory point. The path-following approach is studied in [1], [2], where performance limits for reference-tracking and path-following controllers are investigated and the difference between them is highlighted. It is shown that there is not a fundamental performance limitation for path following for systems with unstable zero dynamics as there is for reference tracking. Building on the work presented in [3] on maneuver modified trajectory tracking, [4] develops an approach that combines the features of trajectory tracking and path following for marine vehicles. Similarly, [5] develops an output maneuvering method composed of two tasks: forcing the output to converge to the desired path and then satisfying a desired speed assignment along the path. The method is demonstrated using a marine vessel simulation. Reference [6] presents a path following method for UAVs that provides a constant line of sight between the UAV and an observation target.

In this paper we will pose the path following problem using the notion of a vector field. The application of vector fields to UAV path following is discussed in [7], [8]. The basic idea is to calculate a desired heading based on the distance from the path. A nice extension of [7] is given in [9] which derives general stability conditions for vector-field based methods. The focus is entirely on orbits, but elongated oval orbits and elliptical orbits can be produced. The method in [9], which is based on Lyapunov techniques, could be extended to straight lines.

The objective of this paper is to develop path following strategies that explicitly account for roll angle and flight path constraints. Previous work has primarily focused on constant altitude maneuvers whereas in this paper we also consider climb maneuver. Our focus will be on following straight-line segments and circular orbits. Our motivation for limiting the focus to these maneuvers is based on the approach described in [10] where straight-line and circular orbits are concatenated to create more sophisticated paths. Straight-line path following is described in Section III, and orbit following will be discussed in Section IV.

## II. Equations of Motion

If $p_n$ and $p_e$ are the inertial North and East position of the vehicle, and $h$ is the altitude, then the kinematic model of the vehicle is given by [10]

$$\dot{p}_n = V_a \cos\psi \cos\gamma_a + w_n \tag{1}$$

$$\dot{p}_e = V_a \sin\psi \cos\gamma_a + w_e \tag{2}$$

$$\dot{h} = V_a \sin\gamma_a + w_h, \tag{3}$$

where $V_a$ is the airspeed, $\psi$ is the heading angle measured from North, $\gamma_a$ is the air mass referenced flight path angle, and $w_n$, $w_e$, and $w_h$ are the North, East, and altitude components of the wind. As explained in [10], using the wind

This research was funded in part by the Air Force Research Laboratory, Munitions Directorate under SBIR contract No. FA 8651-07-C-0094 to Scientific Systems Company, Inc. and Brigham Young University and by NSF award No. CCF-0428004.

R. Beard is a professor in the Electrical and Computer Engineering Department, and J. Humpherys is an associate professor in the Mathematics Department at Brigham Young University, Provo, UT, 84602 USA e-mail: beard@byu.edu, jeffh@math.byu.edu

triangle, an equivalent set of equations is given by

$$\dot{p}_n = V\cos\chi\cos\gamma \tag{4}$$
$$\dot{p}_e = V\sin\chi\cos\gamma \tag{5}$$
$$\dot{h} = V\sin\gamma, \tag{6}$$

where $V$ is the ground speed, $\chi$ is the course angle (angle of the ground track), and $\gamma$ is the inertially referenced flight path angle. The advantage of using this set of equations is that wind does not show up explicitly in the equations and that GPS sensors directly measure $V$, $\chi$, and $\gamma$. The low level autopilot will maintain a constant airspeed, and $V$ is a measured signal.

If we assume coordinated turn conditions, then the equation of motion for the course angle is given by

$$\dot{\chi} = \frac{g}{V}\tan\phi, \tag{7}$$

where $g$ is the gravity constant. We assume in this paper that the roll and pitch dynamics are much faster than the heading and altitude dynamics respectively, which implies that the roll and flight path angles can be considered as the control variables. Therefore Equations (6) and (7) become

$$\dot{h} = V\sin\gamma^c, \tag{8}$$
$$\dot{\chi} = \frac{g}{V}\tan\phi^c, \tag{9}$$

where we will assume that the commanded roll angle is limited by $|\phi^c| \le \phi_{\max}$ and that the commanded flight path angle is limited by $|\gamma^c| \le \gamma_{\max} < \pi/2$.

## III. Straight-Line Path Following

For a straight line path, we will assume that the path is described by two vectors in $\mathbb{R}^3$, namely

$$\mathscr{P}_{\text{line}}(\mathbf{s},\hat{\mathbf{q}}) = \left\{\mathbf{r}\in\mathbb{R}^3 : \mathbf{r} = \mathbf{s} + \alpha\hat{\mathbf{q}}, \alpha\in\mathbb{R}\right\},$$

where $\mathbf{s} = (s_n, s_e, s_d)^T$ is the inertially referenced origin of the path, and $\hat{\mathbf{q}} = (q_n, q_e, q_d)^T$ is a unit vector whose direction indicates the desired direction of travel referenced to the inertial frame. The desired course angle of the path is defined by

$$\chi_{\hat{\mathbf{q}}} \triangleq \tan^{-1}\frac{q_e}{q_n},$$

and the desired flight path angle of the path is defined by

$$\gamma_{\hat{\mathbf{q}}} \triangleq \tan^{-1}\left(\frac{-q_d}{\sqrt{q_n^2+q_e^2}}\right).$$

Figure 1 shows the straight line path $\mathscr{P}_{\text{line}}(\mathbf{s},\hat{\mathbf{q}})$, and the position of the UAV $\mathbf{p}$. The position of the UAV relative to $\mathscr{P}_{\text{line}}$ is given by $\tilde{\mathbf{p}} \triangleq \mathbf{p}-\mathbf{s}$. The heading of the UAV relative to $\mathscr{P}_{\text{line}}$ is given by $\tilde{\chi} = \chi - \chi_{\hat{\mathbf{q}}}$, where $\chi_{\hat{\mathbf{q}}}$ is the inertial heading of $\hat{\mathbf{q}}$ relative to North. To simplify the notation, we express the lateral dynamics in the path frame, where it can be shown that

$$\dot{\tilde{p}}_x = V\cos\tilde{\chi}\cos\gamma \tag{10}$$
$$\dot{\tilde{p}}_y = V\sin\tilde{\chi}\cos\gamma, \tag{11}$$

where $\tilde{p}_x$ is the projected distance along the path and $\tilde{p}_y$ is the cross-track error.

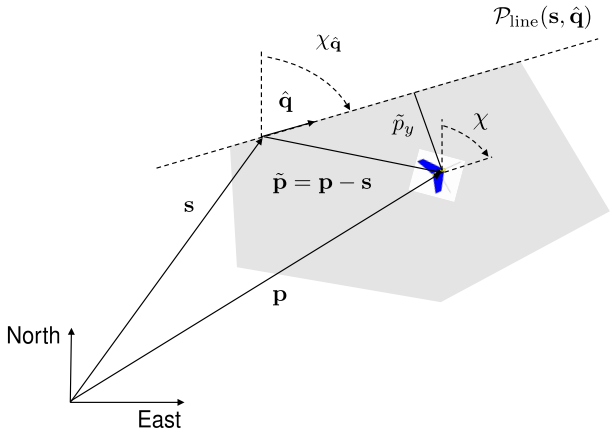


Fig. 1. This figure shows the configuration of the UAV indicated by $(\mathbf{p},\chi)$, and the configuration of the UAV relative to $\mathscr{P}_{\text{line}}$ indicated by $(\tilde{\mathbf{p}},\tilde{\chi})$.

### A. Lateral Guidance Law for Path Following

We will derive the guidance law for following a straight path by decoupling the lateral and longitudinal motion. For the lateral motion we assume that $\gamma$ is a constant. The lateral error dynamics are given by Equations (11) and (9).

Our approach is derived using the theory of nested saturations [11], [12]. The objective is to drive $\tilde{p}_y$ and $\tilde{\chi}$ to zero while simultaneously satisfying the constraint that $|\phi^c| \le \phi_{\max}$. The first step is to differentiate Equation (11) to obtain

$$\ddot{\tilde{p}}_y = g\cos\tilde{\chi}\cos\gamma\tan\phi^c.$$

Define $W_1 = \frac{1}{2}\dot{\tilde{p}}_y^2$ and differentiate to obtain

$$\dot{W}_1 = \dot{\tilde{p}}_y g\cos\tilde{\chi}\cos\gamma\tan\phi^c, \tag{12}$$

and choose

$$\tan\phi^c = -\sigma_{M_1}\left(\frac{k_1\dot{\tilde{p}}_y + \sigma_{M_2}(\zeta)}{g\cos\tilde{\chi}\cos\gamma}\right), \tag{13}$$

where $\sigma_{M_i}$ is the saturation function

$$\sigma_{M_i}(u) \triangleq \begin{cases} M_i, & \text{if } u > M_i \\ -M_i, & \text{if } u < -M_i \\ u, & \text{otherwise} \end{cases},$$

$k_1 > 0$, and $M_1$, $M_2$, and $\zeta$ will be selected in the discussion that follows. Substituting (13) into (12) gives

$$\dot{W}_1 = -\dot{\tilde{p}}_y g\cos\tilde{\chi}\cos\gamma\sigma_{M_1}\left(\frac{k_1\dot{\tilde{p}}_y + \sigma_{M_2}(\zeta)}{g\cos\tilde{\chi}\cos\gamma}\right),$$

which is negative when $|\dot{\tilde{p}}_y| > M_2/k_1$. Therefore, by the ultimate boundedness theorem [13], there exist a time $T_1$ such that for all $t \ge T_1$ we have $|\dot{\tilde{p}}_y| \le M_2/k_1$. If we also select $M_1$ and $M_2$ to satisfy

$$M_1 \ge \frac{2M_2}{g\cos\tilde{\chi}\cos\gamma}, \tag{14}$$

then for all $t \ge T_1$, the signal in $\sigma_{M_1}(\cdot)$ is not in saturation and

$$\dot{W}_1 = -k_1\dot{\tilde{p}}_y^2 - \dot{\tilde{p}}_y\sigma_{M_2}(\zeta). \tag{15}$$

Define $z \triangleq k_1\tilde{p}_y + \dot{\tilde{p}}_y$, and $W_2 = \frac{1}{2}z^2$, and differentiate $W_2$ to obtain

$$\dot{W}_2 = k_1 z\dot{\tilde{p}}_y - zg\cos\tilde{\chi}\cos\gamma\sigma_{M_1}\left(\frac{k_1\dot{\tilde{p}}_y + \sigma_{M_2}(\zeta)}{g\cos\tilde{\chi}\cos\gamma}\right).$$

If we let $\zeta = k_2 z$ where $k_2 > 0$, then for all $t \geq T_1$ we have

$$\begin{aligned}\dot{W}_2 &= k_1 z\dot{\tilde{p}}_y - k_1 z\dot{\tilde{p}}_y - z\sigma_{M_2}(k_2 z)\\ &= -z\sigma_{M_2}(k_2 z),\end{aligned}$$

which is negative definite. Therefore we are guaranteed that $z = k_1\tilde{p}_y + \dot{\tilde{p}}_y \to 0$. Using the standard result on input-to-state stability [13], Equation (15) guarantees that $\dot{\tilde{p}}_y \to 0$. Since both $z = k_1\tilde{p}_y + \dot{\tilde{p}}_y$ and $\dot{\tilde{p}}_y$ converge to zero, we can conclude that $\tilde{p}_y \to 0$.

To ensure that $|\phi|^c \leq \phi_{\max}$, set $M_1 = \tan\phi_{\max}$. To satisfy Equation (14) we also need to constrain $\tilde{\chi}$ and $\gamma$. The constraint on $\gamma$ will be discussed in Section III-B. For $\tilde{\chi}$ note that if $\phi^c = \phi_{\max}$, then $\dot{\tilde{\chi}} = g/V\tan\phi_{\max}$ and $\tilde{\chi}$ increases monotonically. Similarly, if $\phi^c = -\phi_{\max}$, then $\tilde{\chi}$ decreases monotonically. Therefore, if we can find $\tilde{\chi}_{\max}$ such that the set $B_{\tilde{\chi}_{\max}} \triangleq \{|\tilde{\chi}| \leq \tilde{\chi}_{\max}\}$ is positively invariant, then we could use the following strategy for straight line tracking:

$$\phi^c = \begin{cases}\phi_{\max} & \text{if } \tilde{\chi} < -\tilde{\chi}_{\max}\\ -\phi_{\max} & \text{if } \tilde{\chi} > \tilde{\chi}_{\max}\\ -\sigma_{M_1}\left(\frac{k_1\dot{\tilde{p}}_y + \sigma_{M_2}\left(k_2\left(k_1\tilde{p}_y + \dot{\tilde{p}}_y\right)\right)}{g\cos\tilde{\chi}\cos\gamma}\right) & \text{otherwise}\end{cases}. \tag{16}$$

To find $\tilde{\chi}_{\max}$, let $W_3 = \frac{1}{2}\tilde{\chi}^2$ and differentiate to obtain

$$\begin{aligned}\dot{W}_3 &= \frac{g}{V}\tilde{\chi}\tan\phi^c\\ &= -\frac{g}{V}\tilde{\chi}\sigma_{M_1}\left(k_1\frac{V}{g}\tan\tilde{\chi} + \frac{\sigma_{M_2}(k_2 z)}{g\cos\tilde{\chi}\cos\gamma}\right).\end{aligned} \tag{17}$$

Equation (17) is negative if $|k_1 V/g\tan\tilde{\chi}| > |M_2/(g\cos\tilde{\chi}\cos\gamma)|$ which, assuming that $\cos\tilde{\chi} > 0$ and $\cos\gamma > 0$, is true if

$$\sin\tilde{\chi}_{\max} = \frac{M_2}{k_1 V\cos\gamma_{\max}}, \tag{18}$$

where $\gamma_{\max}$ is a parameter that will be specified in the next section.

Since $M_1 = \tan\phi_{\max}$, Equation (14) implies that $M_2$ must be selected so that

$$M_2 \leq \frac{g}{2}\tan\phi_{\max}\cos\tilde{\chi}\cos\gamma.$$

Therefore, we select $M_2$ as

$$M_2 = \frac{g}{2}\tan\phi_{\max}\cos\tilde{\chi}_{\max}\cos\gamma_{\max}.$$

Substituting into Equation (18) we get

$$\tilde{\chi}_{\max} = \tan^{-1}\left(\frac{g}{2k_1 V}\tan\phi_{\max}\right). \tag{19}$$

Therefore we have the following theorem.

*Theorem 3.1:* If the commanded roll angle is given by Equation (16), where

- $k_1 > 0$, $k_2 > 0$,
- $\tilde{\chi}_{\max} = \tan^{-1}\left((g/2k_1 V)\tan\phi_{\max}\right)$,
- $M_1 = \tan\phi_{\max}$,
- $M_2 = \frac{g}{2}\tan\phi_{\max}\cos\tilde{\chi}_{\max}\cos\gamma_{\max}$,

then $\left|\tilde{p}_y(t)\right| + \left|\dot{\tilde{p}}(t)\right| \to 0$, and $|\phi^c(t)| \leq \phi_{\max}$.

### *B. Longitudinal Guidance Law for Path Following*

In this section we develop a longitudinal guidance law for tracking the altitude portion of the waypoint path, where the longitudinal kinematics are given by Equation (8).

The desired altitude for the UAV is found by projecting its current position relative to the waypoint path onto the North-East plane, as shown in Figure 2 and finding the distance to this point which is given by

$$L = \sqrt{\tilde{p}_x^2 + \tilde{p}_y^2}.$$

The position on the waypoint path that, when projected onto the North-East plane, also results in a distance $L$ is given by

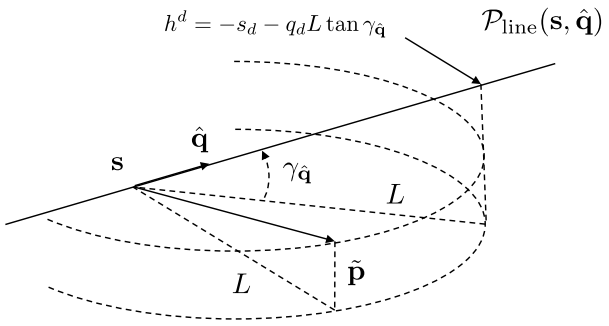


Fig. 2. The desired altitude along the waypoint path is found by projecting the position error of the UAV onto the North-East plane. The length of the projection $L$ is used to find the point on the waypoint path that also projects onto the North-East plane a distance $L$ from $\mathbf{s}$ and using the altitude at that point.

$$\mathbf{z} = \mathbf{s} + \hat{\mathbf{q}}L\tan\gamma_{\hat{\mathbf{q}}}.$$

The down component of this vector is used to obtain the desired altitude as

$$h^d = -s_d - q_d L\tan\gamma_{\hat{\mathbf{q}}}. \tag{20}$$

The time derivative of $h^d$ is given by

$$\dot{h}^d = -q_d\tan\gamma_{\hat{\mathbf{q}}}V\frac{\tilde{p}_x\cos\chi\cos\gamma + \tilde{p}_y\sin\chi\cos\gamma}{\sqrt{\tilde{p}_x^2 + \tilde{p}_y^2}}. \tag{21}$$

Define $W_4 = \frac{1}{2}(h - h^d)^2$ and differentiate to obtain

$$\begin{aligned}\dot{W}_4 &= (h - h^d)(\dot{h} - \dot{h}^d)\\ &= (h - h^d)(V\sin\gamma^c - \dot{h}^d).\end{aligned}$$

If we select $\gamma^c$ so that

$$V\sin\gamma^c - \dot{h}^d = -\sigma_{M_3}\left(k_3(h - h^d)\right),$$

or in other words

$$\gamma^c = \sin^{-1}\left(\frac{\dot{h}^d - \sigma_{M_3}\left(k_3(h - h^d)\right)}{V}\right), \tag{22}$$

then $\dot{W}_4 = -(h-h^d)\sigma_{M_3}\left(k_3(h-h^d)\right)$ is negative definite.

To ensure that $|\gamma^c| \leq \gamma_{\max}$, note that

$$\begin{aligned}\left|\dot{h}^d\right| &= \left|-q_d \tan\gamma_{\hat{\mathbf{q}}} V \frac{\tilde{p}_x \cos\chi\cos\gamma + \tilde{p}_y \sin\chi\cos\gamma}{\sqrt{\tilde{p}_x^2+\tilde{p}_y^2}}\right| \\ &= V\left|\tan\gamma_{\hat{\mathbf{q}}}\right| \frac{|\tilde{p}_x|+|\tilde{p}_y|}{\sqrt{\tilde{p}_x^2+\tilde{p}_y^2}} \\ &= \sqrt{2}V\left|\tan\gamma_{\hat{\mathbf{q}}}\right|,\end{aligned}$$

where we have used the fact that $\|\hat{\mathbf{q}}\| = 1$ implies that $|q_d| \leq 1$, and the fact that $\|\cdot\|_1 \leq \sqrt{2}\|\cdot\|_2$. Therefore

$$\begin{aligned}\left|\frac{\dot{h}^d - \sigma_{M_3}\left(k_3(h-h^d)\right)}{V}\right| &\leq \frac{\left|\dot{h}^d\right|}{V} + \frac{M_3}{V} \\ &\leq \sqrt{2}\left|\tan\gamma_{\hat{\mathbf{q}}}\right| + \frac{M_3}{V}.\end{aligned}$$

If $M_3$ is selected as

$$M_3 = V\sin\gamma_{\max} - \sqrt{2}V\left|\tan\gamma_{\hat{\mathbf{q}}}\right|, \tag{23}$$

then from Equation (22) we have that $|\gamma^c| \leq \gamma_{\max}$. To ensure that $M_3 > 0$ we require that $\gamma_{\max}$ and $\gamma_{\hat{\mathbf{q}}}$ satisfy

$$\sin\gamma_{\max} > \sqrt{2}\left|\tan\gamma_{\hat{\mathbf{q}}}\right|. \tag{24}$$

Theorem 3.2 summarizes the results.

*Theorem 3.2:* If the flight path angle of the waypoint path satisfies Equation (24), and if the commanded flight path angle is given by Equation (22), where $k_3 > 0$, $\dot{h}^d$ is given by Equation (21), and $M_3$ is given by Equation (23), then $h \to h^d$ and $|\gamma^c(t)| \leq \gamma_{\max}$, for all $t \geq 0$.

## IV. Orbit Following

Alternatively, an orbital path is described by an inertially referenced center $\mathbf{c} = (c_n, c_e, c_d)^T$, a radius $\rho \in \mathbb{R}$, and a direction $\lambda \in \{-1, 1\}$, as

$$\begin{aligned}&\mathscr{P}_{\text{orbit}}(\mathbf{c},\rho,\lambda) = \\ &\left\{\mathbf{r} \in \mathbb{R}^3 : \mathbf{r} = \mathbf{c} + \lambda\rho\begin{pmatrix}\cos\varphi, & \sin\varphi & 0\end{pmatrix}^T, \varphi \in [0, 2\pi)\right\},\end{aligned}$$

where $\lambda = 1$ signifies a clockwise orbit and $\lambda = -1$ signifies a counterclockwise orbit.

The guidance strategy for orbit following is best derived in polar coordinates. Let

$$d \triangleq \sqrt{(p_n - c_n)^2 + (p_e - c_e)^2}$$

be the lateral distance from the desired center of the orbit to the UAV, and let

$$\varphi \triangleq \tan^{-1}\left(\frac{p_e - c_e}{p_n - c_n}\right) \tag{25}$$

be the phase angle of the relative position, as shown in Figure 3. Differentiating $d$ and using Equations (4) and (5) gives

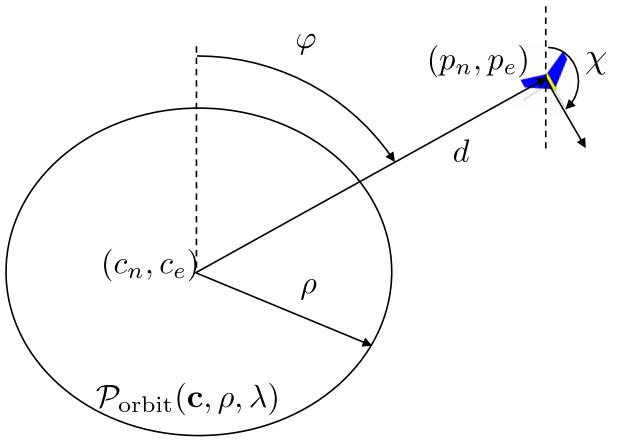


Fig. 3. Conversion from rectangular coordinates to polar coordinates for orbit following.

$$\begin{aligned}\dot{d} &= \frac{(p_n - c_n)\dot{p}_n + (p_e - c_e)\dot{p}_e}{d} \\ &= \frac{(p_n - c_n)V\cos\chi\cos\gamma + (p_e - c_e)V\sin\chi\cos\gamma}{d}.\end{aligned}$$

Using Equation (25) gives

$$\begin{aligned}\dot{d} &= V\cos\gamma\frac{(p_n - c_n)\cos\chi + (p_e - c_e)\sin\chi}{d} \\ &= V\cos\gamma\left(\frac{p_n - c_n}{d}\right)(\cos\chi + \sin\chi\tan\varphi) \\ &= V\cos\gamma\cos\varphi\,(\cos\chi + \sin\chi\tan\varphi) \\ &= V\cos\gamma(\cos\chi\cos\varphi + \sin\chi\sin\varphi) \\ &= V\cos\gamma\cos(\chi - \varphi).\end{aligned}$$

Similarly, differentiating Equation (25) and simplifying gives

$$\dot{\varphi} = \frac{V\cos\gamma}{d}\sin(\chi - \varphi).$$

The orbital kinematics in polar coordinates are therefore given by

$$\begin{aligned}\dot{d} &= V\cos(\chi - \varphi)\cos\gamma \\ \dot{\varphi} &= \frac{V}{d}\sin(\chi - \varphi)\cos\gamma \\ \dot{\chi} &= \frac{g}{V}\tan\phi^c.\end{aligned}$$

As shown in Figure 4, for a clockwise orbit, the desired course angle when the UAV is located on the orbit is given by $\chi^d = \varphi + \pi/2$. Similarly, for a counterclockwise orbit, the desired angle is given by $x^d = \varphi - \pi/2$. Therefore, in general we have

$$x^d = \varphi + \lambda\frac{\pi}{2}.$$

Defining the error variables $\tilde{d} \triangleq d - \rho$ and $\tilde{\chi} \triangleq \chi - \chi^d$, the orbital kinematics can be restated as

$$\dot{\tilde{d}} = -\lambda V\sin\tilde{\chi}\cos\gamma \tag{26}$$

$$\dot{\tilde{\chi}} = \frac{g}{V}\tan\phi^c - \lambda\frac{V}{\tilde{d}+\rho}\cos\tilde{\chi}\cos\gamma. \tag{27}$$

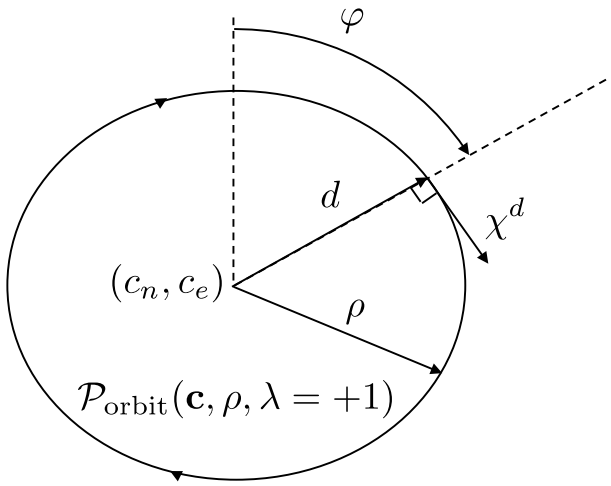


Fig. 4. The desired angle when the UAV is on the orbit is given by $\chi^d$.

The control objective is to drive $\tilde{d}(t) \to 0$, $\tilde{\chi}(t) \to 0$, while satisfying the input constraint $|\phi^c(t)| \leq \phi_{\max}$.

Our approach to developing the orbit following guidance strategy is similar to the method followed in Section III-A with the added complication that we must deal with the inside of the orbit.

Following the exposition in Section III-A, differentiate Equation (26) to obtain

$$\begin{aligned}\ddot{\tilde{d}} &= -\lambda V \cos\tilde{\chi}\cos\gamma\dot{\tilde{\chi}} \\ &= -\lambda g V \cos\gamma\cos\tilde{\chi}\left(\frac{g}{V}\tan\phi^c - \lambda\frac{V}{d}\cos\gamma\cos\tilde{\chi}\right) \\ &= -g\cos\gamma\cos\tilde{\chi}\left(\lambda\tan\phi^c - \frac{V^2}{g(\tilde{d}+\rho)}\cos\gamma\cos\tilde{\chi}\right).\end{aligned}$$

Define $W_5 = \frac{1}{2}\dot{\tilde{d}}^2$ and differentiate to obtain

$$\dot{W}_5 = -\dot{\tilde{d}}\lambda g\cos\gamma\cos\tilde{\chi}\left(\tan\phi^c - \lambda\frac{V^2}{g(\tilde{d}+\rho)}\cos\gamma\cos\tilde{\chi}\right). \tag{28}$$

and choose $\phi^c$ so that

$$\phi_c = \tan^{-1}\left[\lambda\frac{V^2}{gd}\cos\gamma\cos\tilde{\chi} + \lambda\sigma_{M_4}\left(\frac{k_4\dot{\tilde{d}} + \sigma_{M_5}(\zeta)}{g\cos\gamma\cos\tilde{\chi}}\right)\right], \tag{29}$$

where $k_4 > 0$ is a control gain, and $M_4$, $M_5$, and $\zeta$ will be selected in the following discussion. Substituting Equation (29) into Equation (28) gives

$$\dot{W}_5 = -\dot{\tilde{d}}g\cos\tilde{\chi}\cos\gamma\sigma_{M_4}\left(\frac{k_4\dot{\tilde{d}} + \sigma_{M_5}(\zeta)}{g\cos\gamma\cos\tilde{\chi}}\right),$$

which is negative when $\left|\dot{\tilde{d}}\right| > M_5/k_4$. Therefore, by the ultimate boundedness theorem [13] there exists a time $T_3$ such that for all $t \geq T_3$, we have $\left|\dot{\tilde{d}}\right| \leq M_5/k_4$. If we select $M_4$ and $M_5$ to satisfy

$$M_4 \geq \frac{2M_5}{g\cos\tilde{\chi}\cos\gamma}, \tag{30}$$

then for all $t \geq T_3$, the signal $\sigma_{M_4}$ is not in saturation and

$$\dot{W}_5 = -k_4\dot{\tilde{d}}^2 - \dot{\tilde{d}}\sigma_{M_5}(\zeta). \tag{31}$$

Define $z_2 = k_4\tilde{d} + \dot{\tilde{d}}$ and $W_6 = \frac{1}{2}z_2^2$, and differentiate $W_6$ to obtain

$$\dot{W}_6 = z_2 k_4\dot{\tilde{d}} - z_2 g\cos\gamma\cos\tilde{\chi}\sigma_{M_4}\left(\frac{k_4\dot{\tilde{d}} + \sigma_{M_5}(\zeta)}{g\cos\gamma\cos\tilde{\chi}}\right). \tag{32}$$

If we let $\zeta = k_5 z_2$, where $k_5 > 0$ is a control gain, then for all $t \geq T_3$ we have

$$\dot{W}_6 = -z_2\sigma_{M_5}(k_5 z_2),$$

which is negative definite. Therefore we are guaranteed that $z_2 = k_4\tilde{d} + \dot{\tilde{d}} \to 0$. Using the standard result on input-to-state stability [13], Equation (31) guarantees that $\dot{\tilde{d}} \to 0$. We can therefore conclude that $\tilde{d} \to 0$.

To satisfy the input saturation constraint, from Equation (29) we require that

$$\tan\phi_{\max} \geq \frac{V^2}{dg}|\cos\gamma|\,|\cos\tilde{\chi}| + M_4.$$

If we ensure that when Equation (29) holds, that $d \geq d_{\min}$ and that $|\tilde{\chi}| \leq \tilde{\chi}_{\max}$, then a sufficient condition to avoid input saturation is that

$$\tan\phi_{\max} \geq \frac{V^2}{d_{\min}g}\cos\gamma_{\max}\cos\tilde{\chi}_{\max} + M_4.$$

Therefore, select

$$M_4 = \tan\phi_{\max} - \frac{V^2}{d_{\min}g}\cos\gamma_{\max}\cos\tilde{\chi}_{\max}, \tag{33}$$

where, to ensure that $M_4 > 0$ we require that $\phi_{\max}$, $d_{\min}$, $\tilde{\chi}_{\max}$ be selected so that

$$\tan\phi_{\max} > \frac{V^2}{d_{\min}g}\cos\gamma_{\max}\cos\tilde{\chi}_{\max}. \tag{34}$$

To satisfy constraint (30) select $M_5$ as

$$M_5 = \frac{1}{2}M_4 g\cos\tilde{\chi}_{\max}\cos\gamma_{\max}. \tag{35}$$

From Equation (34) we see that the control strategy (29) can only be active when $|\tilde{\chi}| \leq \tilde{\chi}_{\max}$ and $d \geq d_{\min}$. The basic strategy will be to command a zero roll angle when $d < d_{\min}$ and to saturate the roll angle at $\pm\phi_{\max}$ when $|\tilde{\chi}| > \tilde{\chi}_{\max}$ in the direction that reduces $|\tilde{\chi}|$. Therefore, let

$$\phi^c = \begin{cases} 0 & \text{if } d < d_{\min} \\ -\lambda\phi_{\max} & \text{if } (d \geq d_{\min}) \text{ and } (\lambda\tilde{\chi} \geq \tilde{\chi}_{\max}) \\ \lambda\phi_{\max} & \text{if } (d \geq d_{\min}) \text{ and } (-\lambda\tilde{\chi} \geq \tilde{\chi}_{\max}) \\ [\text{Equation (29)}] & \text{otherwise} \end{cases}. \tag{36}$$

The convergence result is summarized in the following theorem

*Theorem 4.1:* If the commanded roll angle is given by Equation (36) where

- $k_4 > 0$,
- $\phi_{\max}$, $\gamma_{\max}$, and $\tilde{\chi}_{\max}$ are positive and less than $\pi/2$,

- $0 < d_{\min} < \rho$
- $M_4$ is given by Equation (33)
- $M_5$ is given by Equation (35)

then $|\phi^c(t)| \leq \phi_{\max}$, and $(d, \tilde{\chi}) \to (\rho, 0)$.

## V. Conclusion

This paper has considered the problem of following straight-lines and orbits using fixed wing unmanned air vehicles where the roll angle and flight path constraints are explicitly taken into account. The guidance strategies are derived using a kinematic model of the aircraft and using the theory of nested saturations. The resulting strategies are continuous and computationally simple.

## References


[1] P. Aguiar, D. Dačić, J. Hespanha, and P. Kokotović, "Path-following or reference-tracking? An answer relaxing the limits to performance," in *Proceedings of IAV2004, 5th IFAC/EURON Symposium on Intelligent Autonomous Vehicles*, Lisbon, Portugal, 2004.

[2] A. P. Aguiar, J. P. Hespanha, and P. V. Kokotovic, "Path-following for nonminimum phase systems removes performance limitations," *IEEE Transactions on Automatic Control*, vol. 50, no. 2, pp. 234–238, February 2005.

[3] J. Hauser and R. Hindman, "Maneuver regulation from trajectory tracking: Feedback linearizable systems," in *Proceedings of the IFAC Symposium on Nonlinear Control Systems Design*, Tahoe City, CA, June 1995, pp. 595–600.

[4] P. Encarnação and A. Pascoal, "Combined trajectory tracking and path following: An application to the coordinated control of marine craft," in *Proceedings of the IEEE Conference on Decision and Control*, Orlando, FL, 2001, pp. 964–969.

[5] R. Skjetne, T. Fossen, and P. Kokotović, "Robust output maneuvering for a class of nonlinear systems," *Automatica*, vol. 40, pp. 373–383, 2004.

[6] R. Rysdyk, "UAV path following for constant line-of-sight," in *Proceedings of the AIAA 2nd Unmanned Unlimited Conference*. AIAA, September 2003, paper no. AIAA-2003-6626.

[7] D. R. Nelson, D. B. Barber, T. W. McLain, and R. W. Beard, "Vector field path following for miniature air vehicles," *IEEE Transactions on Robotics*, vol. 37, no. 3, pp. 519–529, June 2007.

[8] ——, "Vector field path following for small unmanned air vehicles," in *American Control Conference*, Minneapolis, Minnesota, June 2006, pp. 5788–5794.

[9] D. A. Lawrence, E. W. Frew, and W. J. Pisano, "Lyapunov vector fields for autonomous unmanned aircraft flight control," in *AIAA Journal of Guidance, Control, and Dynamics*, vol. 31, no. 5, September-October 2008, pp. 1220–12 229.

[10] R. W. Beard and T. W. McLain, *Small Unmanned Aircraft: Theory and Practice*. Princeton University Press, 2011 (to appear).

[11] P. Castillo, R. Lozano, and A. E. Dzul, *Modelling and Control of Mini-Flying Machines*. Springer, 2005.

[12] A. R. Teel, "Global stabilization and restricted tracking for multiple integrators with bounded controls," *Systems & Control Letters*, vol. 18, no. 3, pp. 165–171, March 1992.

[13] H. K. Khalil, *Nonlinear Systems*, 3rd ed. Upper Saddle River, NJ: Prentice Hall, 2002.